Cortical excitation:inhibition imbalance causes network-specific functional hypoconnectivity: a DREADD-fMRI study

Authors: Marija Markicevic [a], Ben D. Fulcher [b], Christopher Lewis [c], Fritjof Helmchen [c,d], Markus Rudin[d,e,f], Valerio Zerbi* [a,d] and Nicole Wenderoth* [a,d].

[a] Neural Control of Movement Lab, HEST, ETH Zürich, Winterthurerstrasse 190, 8057 Zurich, Switzerland

[b] Complex Systems Group, School of Physics, Faculty of Science, University of Sydney, Australia

[c] Brain Research Institute, University of Zurich, Winterthurerstrasse 190, 8057 Zurich, Switzerland

[d] Neuroscience Center Zurich, University and ETH Zurich, Winterthurerstrasse 190, 8057 Zurich, Switzerland

[e] Institute of Pharmacology and Toxicology, University of Zurich, Winterthurerstrasse 190, 8057 Zurich, Switzerland

[f] Institute for Biomedical Engineering, University and ETH Zurich, Wolfgang-Pauli-Str. 27, 8093 Zurich, Switzerland

* V.Z and N.W share last authorship.

Corresponding author:

Dr. Valerio Zerbi

Neural Control of Movement Lab

Department of Health Sciences and Technology

ETH Zürich, Switzerland

Winterthurerstrasse 190, 8057 Zürich

Phone: +41 44 63 56101

valerio.zerbi@hest.ethz.ch

Short/Running title: Hypo-connectivity explained by neuronal hyper-excitability

Abbreviations

ASL – arterial spin labelling

BOLD – blood-oxygen level dependent

CAMKII – alpha-calcium/calmodulin-dependent protein kinase II promoter

CBF – cerebral blood flow

CP – caudate putamen

DREADD – Designer Receptors Exclusively Activated by Designer Drugs

FC – functional connectivity

hM3Dq – excitatory DREADD

hM4Di – inhibitory DREADD

MOctx – primary somatomotor cortex

PV – parvalbumin interneurons

PVCre –parvalbumin cre-dependant

PVCre-hM4Di – PVCre mice injected with hM4Di DREADD

ReHo – Regional Homogeneity

rsfMRI – resting-state functional Magnetic Resonance Imaging

SSctx – primary somatosensory cortex

STR – striatum

TEa – temporal association cortex

TH – thalamus

VMHC – Voxel-mirrored Homotopic Connectivity

Wt-hM3Dq – wildtype mice injected with hM3Dq DREADD

Abstract

Resting-state fMRI (rsfMRI) is a widespread method utilized for estimating brain-wide functional connectivity (FC) in health and disease. However, the cellular underpinnings of aberrant FC detected in numerous neuropsychiatric conditions in humans and animal models remain unknown. Here we altered the neural dynamics within cortical microcircuits such that excitation:inhibition (E:I) ratio increases and tested whether this manipulation causes abnormal FC at the macroscopic level. Using a mouse model, we combined functional magnetic resonance at the resting state (rsfMRI) with Designer Receptors Exclusively Activated by Designer Drugs (DREADDs) to (i) locally increase excitation using hM3Dq-DREADDs, or (ii) locally suppress activity of inhibitory Parvalbumin interneurons with hM4Di-DREADDs in the somatosensory network. Irrespective of which pathway was used to increase the E:I ratio, activating the DREADDs significantly increased neuronal firing and relative blood flow around the injection site and caused a rapid and long-lasting reduction in local and long-range FC. We further show that both DREADD manipulations change the BOLD dynamics of the injection site in a similar manner suggesting that an increase of E:I converges on a common BOLD timeseries signature. Our approach represents the first steps towards identifying a causal link between E:I at the cellular-population level and brain-wide, macroscopic functional connectivity, the latter being an important marker of neurodevelopmental disorders which translates across species.

1. Introduction

Complex behavior results from the interplay of specialized brain circuits formed by spatially distributed yet anatomically connected neuronal populations. The brain-wide organization of these circuits has been frequently studied by applying functional Magnetic Resonance Imaging during the resting state (rsfMRI). RsfMRI is a measurement commonly used to construct statistical correlations between spontaneous, slow-frequency fluctuations in the blood oxygen level-dependent (BOLD) signals (Mateo et al., 2017), often referred to as functional connectivity (FC). It has been hypothesized that these BOLD fluctuations reflect infra-slow neural dynamics (Mitra et al., 2018) and power fluctuations of gamma frequency neural rhythms (Fox and Raichle, 2007, Lewis et al., 2016) which phase-lock within and across neuronal ensembles, indicating that activity modulations of these populations follow similar temporal patterns.

A large body of research has shown that FC derived from rsfMRI is largely contingent on structural connectivity (Grandjean et al., 2017b, Greicius et al., 2009, Hagmann; et al., 2008). Moreover, FC architecture predicts individual differences in task-dependent activity (Tavor; et al., 2018) and is sensitive to neuropsychiatric conditions in both human patients (Di Martino et al., 2014, Alaerts et al., 2014, Balsters et al., 2017) and mouse models of brain disorders (M. G. Haberl et al., 2015, Zerbi et al., 2018a, Bertero et al., 2018). These properties have contributed to rsfMRI becoming an increasingly popular measurement in clinical populations (Kraguljac et al., 2016, Kennedy and Adolphs, 2012, Kahan et al., 2014) and for translational research (Grayson et al., 2016, Zerbi et al., 2018b, Liska et al., 2018, Sforazzini et al., 2016, Lazaro and Golshani, 2015). Interestingly, patients with Autism Spectrum Disorder (ASD) and genetically manipulated mouse models mimicking this condition display similar aberrations of long-range connectivity in plausible mouse-human homologue networks, suggesting a mechanistic link between genetic risk for neurodevelopmental disorders and long-range functional decoupling (Liska et al., 2018, Scott-Van Zeeland et al., 2010, Zerbi et al., 2018b, Bertero et al., 2018). However, the cellular underpinnings of these observations are currently largely unknown. One hypothesis proposes that FC alterations reflect an abnormal excitation:inhibition (E:I) balance within cortical microcircuits (Rubenstein and Merzenich, 2003, Lewis et al., 2012). In the healthy brain, excitation of pyramidal cells causes a proportional increase of inhibition by recruiting inhibitory cortical neurons (Mingshan et al., 2014, Okun and Lampl, 2008), a mechanism which is finely tuned to ensure the efficiency of cortical information processing (Isaacson and Scanziani, 2011, Vogels et al., 2011, Haider and Mccormick, 2009). Growing evidence supports a fundamental role of fast-spiking parvalbumin (PV) GABAergic interneurons in maintaining the E:I balance by acting as an essential regulator of synchronized activity (Packer and Yuste, 2011). Further, their function is heavily diminished in numerous psychiatric diseases, including schizophrenia and autism and their expression is reduced in many relevant animal models including CNTNAP2, FMR1, En2 and Shank3 knock-out mice (Penagarikano et al., 2011, Vogt et al., 2017,

Wohr et al., 2015). This results in over-excitation of neocortex, which has been associated with spontaneous recurrent seizures, hyperactivity and impaired neural signaling (Penagarikano et al., 2011, Ajram et al., 2017).

Here we investigate whether this state of unsynchronized over-excitation within cortical circuits can cause long-range *hypo*-connectivity as previously detected by rsfMRI in these same animal models (Liska et al., 2018, Zerbi et al., 2018b, Pagani et al., 2018). We aimed at providing direct causal evidence that shifting the E:I balance of a brain region towards excitation results in a significant FC decrease with other brain regions. Designer Receptors Exclusively Activated by Designer Drugs (DREADDs) (Michaelides and Hurd, 2016, Rogan and Roth, 2011) were used to experimentally manipulate the cortical E:I balance, while simultaneously monitoring alterations in FC across the entire mouse brain by rsfMRI (Zerbi et al., 2015, Grandjean et al., 2017a). Specifically, we increased cortical excitation via two different mechanisms: (i) net neuronal excitability was increased by expressing depolarizing DREADDs in cortical neurons of wildtype mice (wt-hM3Dq); or (ii) GABAergic PV interneurons were suppressed via hyperpolarizing DREADDs in PVCre mice (PVCre-hM4Di). We show that both interventions increase the E:I ratio at the microcircuit level and lead to similar perturbations in BOLD fluctuation patterns which cause *hypo*-connectivity between remote yet structurally connected areas at the macroscale.

2. Results

Adult, male C57BL/6 mice were either transfected with excitatory DREADD in the right somatosensory cortex (SSctx) (wt-hM3Dq, $n = 10$) or were sham operated (weight and age-matched littermate controls, $n = 9$; Fig. 1A). For additional information see Suppl. Table S1. Three to four weeks after surgery, mice underwent two scanning sessions separated by at least one week, in which we measured how activating the DREADDS influenced cerebral blood flow (CBF) and rsfMRI (Fig. 1B), respectively. In both sessions, we kept the mice under light isoflurane+medetomidine anesthesia (see methods) and recorded 15 min of baseline, before activating the DREADDs with clozapine (0.01-0.03mg/kg, i.v.). After clozapine injection, we continued the recordings for 45 minutes. Note that early experiments used clozapine-N-oxide (CNO) to activate DREADDs. However, recent literature reported that DREADDs are strongly activated by clozapine, a metabolite of CNO, which unlike CNO crosses the blood-brain barrier and has a high affinity for DREADD receptors at low doses (Gomez et al., 2017, Manvich et al., 2018). To ensure controlled DREADD activation and reduce the risk of unspecific binding, we used very low doses of clozapine (<0.05 mg/kg); however, we also scanned a small cohort of mice using CNO, which revealed analogous results (Suppl. Fig. S3). Once the scanning was completed, mice were euthanized and immunohistochemical analyses confirmed a strong viral expression in the primary somatosensory cortex in all wt-hM3Dq mice (Suppl. Fig. S5).

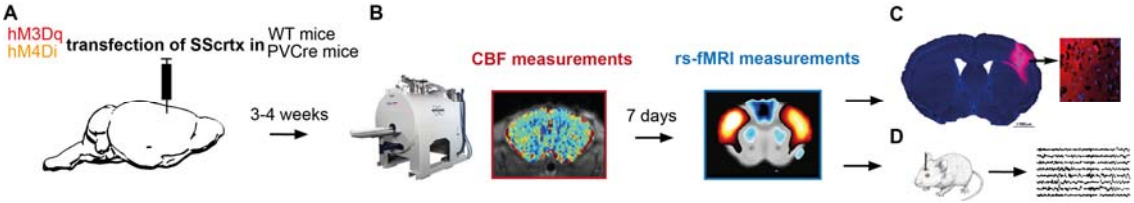

Figure 1. Scheme of the experimental pipeline. A) *Administration of hM3Dq or DIO-hM4Di DREADDs constructs via viral injection into the right primary somatosensory cortex of wildtype and PVCre mice, respectively.* ***B)*** *Three to four weeks after surgery, mice underwent multi-modal MRI functional imaging for the assessment of cerebral blow flow and resting-state fMRI. In each session, clozapine is injected i.v. (<0.05 mg/kg) during the recordings to activate the DREADDs.* ***C)*** *After the MRI, the successful viral transfection is ensured by immunohistochemistry. Figure depicts results from a single brain slice.* ***D)*** *In vivo electrophysiology recordings are taken from the right primary somatosensory cortex and from a control region, to confirm that DREADD transfected neurons are successfully and selectively activated after clozapine injection and cause a net shift towards over-excitation.*

2.1 *In vivo* electrophysiology

In order to confirm that hM3Dq-DREADD caused modulation of neural activity in the targeted region, we performed *in vivo* electrophysiology recordings under isoflurane anaesthesia (0.5%) (Alexander et al., 2009). Multi-unit activity was recorded from multi-contact electrode arrays at the injection site in the right SSctx and its homotopic counterpart, left SSctx, in wt-hM3Dq mice. During the baseline period (15 minutes) the average basal firing rate remained stable, while upon clozapine injection the average firing rate in the right SSctx increased steadily over time. Multiunit activity recorded in the left SSctx remained virtually unchanged before and after the clozapine injection. At 30 min, the difference between the left and the right SSctx reached 11% (Fig. 2A-D).

2.2 Activation of hM3Dq-DREADD drives a local increase of blood perfusion at the injection site indicating enhanced neural firing

We used non-invasive MRI to test whether activation of hM3Dq-DREADD would elicit an increase in local blood perfusion. After administering clozapine, wt-hM3Dq mice showed an increase in cerebral blood flow (CBF) relative to baseline around the injection site (Fig. 2E, H). This increase was higher than in sham operated mice (controls) undergoing the identical scanning procedure (Fig. 2F, I). The increase in CBF in the wt-hM3Dq mice relative to the controls was significant for all time points up to 45 min after clozapine injection (Linear mixed model: $F_{2,21}$=5.657, p = 0.04). No such changes of CBF were observed in non-injected control regions, i.e., the contralateral somatosensory cortex nor in the ipsilateral striatum (Fig. 2J, K). These results show that activating hM3Dq DREADD increases CBF specifically in the injected area, but not in anatomically connected transcallosal or ipsilateral regions.

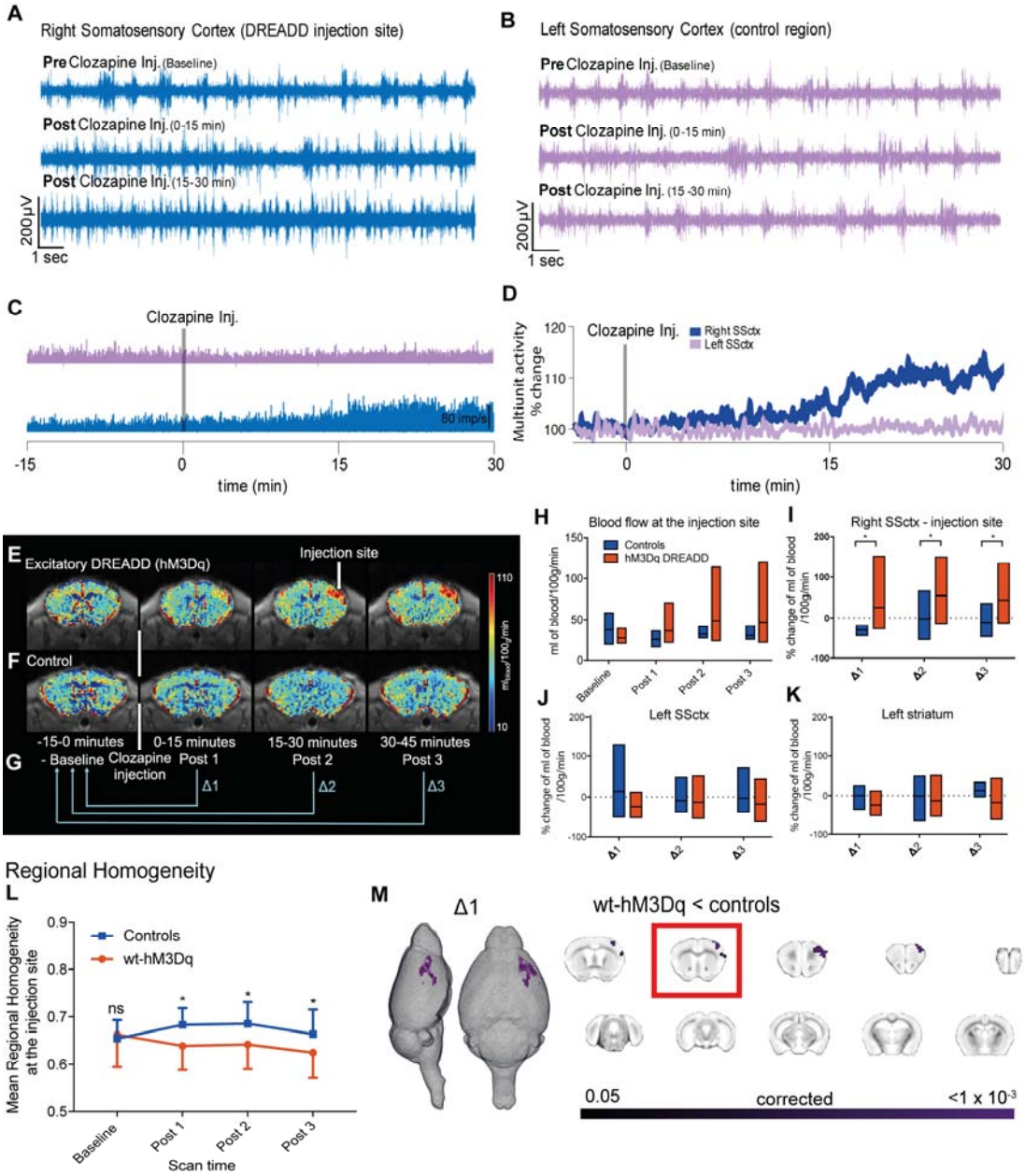

Figure 2. Local changes induced by activating hM3Dq. A) *Figure depicts neuronal firing rate before and after clozapine injection at the right somatosensory cortex (SSctx) (ie. DREADD injection site), indicating a steady increase in firing rate upon DREADD activation.* ***B)*** *As A but for the left somatosensory cortex, indicating no change of the neuronal firing rate after clozapine injection.* ***C)*** *Time-resolved firing rate in millisecond bins for the right (blue) and left (violet) somatosensory cortices. A steady increase of firing rate occurs at the right SSctx once clozapine is injected (upon 15 minutes of the baseline recording), while no change occurs at the left SSctx.* ***D)*** *Averaged multiunit activity increased by 11% compared to the baseline (pre-clozapine injection) at the right SSctx and remained similar to the baseline at the left SSctx* ***E), F)*** *Cerebral blood flow maps are collected every 15 minutes for an wt-hM3Dq mouse and a control mouse, respectively.* ***G)*** *Clozapine injection occurs 15 minutes after the start of experiment, this is referred as the baseline period and referred to as -15-0 min. The rest of the experiment is 45 minutes long and divided into 3 periods i.e., Post 1 (0-15 min), Post 2 (15-30 min)*

and Post 3 (30-45 min). For all the analysis performed in this experiment (unless otherwise stated), all the data has been normalized (Post 1/Post 2/Post 3 – baseline) which refer to Δ1, Δ2, Δ3, respectively. ***H)*** *Comparison of blood flow (ml of blood/100g/min) between controls and wt-hM3Dq mice over time as measured at the injection site.* ***I)*** *Percentage change of blood flow over time between the controls and wt-hM3Dq mice as measured at the injection site. Linear mixed models indicate a significant main group effect indicating an increase of blood flow in the wt-hM3Dq mice (F(2,21)=5.657; p=0.04).* ***J)*** *as measured at left somatosensory cortex* ***K)*** *as measured at left lateral striatum.* ***L)*** *Change over time of the mean regional homogeneity (ReHo) at the injection site. Repeated measures ANOVA showed a significant interaction between the scan time and groups (F(1.93,75)=11.8; p=0.000).* ***M)*** *Corrected significant decrease in regional homogeneity depicted as 3D image for Δ1, and shown through coronal slices for Δ1 time point. The slice marked with a red rectangle is the injection slice.*

2.3 Activating hM3Dq-DREADD decreases short-range connectivity selectively within somatosensory and somatomotor cortex

We then tested whether hM3Dq-DREADD would also cause a disruption of short-range functional connectivity within the injected region. To this end, we measured regional homogeneity (ReHo) from the rsfMRI data, a commonly used metric to assess the statistical dependencies of the BOLD time courses measured in neighbouring voxels which reflects the level of local synchronization between rsfMRI signals (Zang et al., 2004). ReHo has been used to detect alterations occurring in various psychiatric diseases including depression, schizophrenia, and autism (Paakki et al., 2010, Iwabuchi et al., 2015). Activation of hM3Dq-DREADDs significantly reduced ReHo in the right SSctx (the injection site) and in the neighbouring, densely connected somatomotor cortex, in wt-hM3Dq mice as compared to controls (blue cluster in Fig. 2 L, M; $p<0.05$, TFCE-corrected). These changes occurred during the first 15 minutes after clozapine injection and were maintained throughout the entire scan time of 45 minutes (Suppl. Fig. S2A).

2.4 HM3Dq DREADD reduces functional connectivity between somatosensory cortex and monosynaptically connected cortical areas

Does an increase of neuronal excitability also affect long-range FC? To address this question, we looked at changes in FC within the *somatosensory network*. This network is defined as the ensemble of tracer-based anatomical projections from the SSctx to the rest of the brain according to the Allen Mouse Brain Connectivity atlas (Oh et al., 2014) and includes contralateral primary SSctx, bilateral somatomotor cortex (MOctx), bilateral association areas (TEa), as well as ipsilateral caudatum putamen (CP) and thalamus (TH; Parafascicular nucleus) (Fig. 3A). All these structures exhibited high FC among each other when assessed during baseline (Fig. 3B). This structure-function correspondence confirms that the somatosensory network is an excellent anatomical model to test how E:I imbalance of a single region affects FC in downstream, monosynaptically connected areas.

FC matrices were determined as Pearson's correlations of BOLD time series for 15 min blocks before (baseline) and after injection of clozapine (three 15 min post-measurements) (Fig. 3C, D, E and suppl. Fig. 1A). Baseline FC was similar between groups (Fig. 3C). By contrast, after clozapine injection (Fig. 3D-F), we observed a reduction in FC between right SSctx and nearly all other areas of the network in wt-hM3Dq mice. Significant group differences (randomized permutation testing, $p < 0.05$, FDR corrected) were found between right SSctx and left SSctx /left MOctx, as well as between left and right MOctx, and were maintained throughout the whole scan session (Fig. 3F, Suppl. Fig. S1B).

Finally, we investigated if the observed FC perturbations are specific to the somatosensory cortices or whether they also affect other brain regions or networks. We first analysed Voxel-Mirrored Homotopic Connectivity (VMHC), a simple metric that measures the similarity between the BOLD time series of any pair of symmetric inter-hemispheric voxels. This index has been shown to identify pathological connectivity patterns with high sensitivity (Hahamy et al., 2015). In line with our previous findings, injecting clozapine caused a significant reduction of VMHC between the primary left and right SSctx as well as the left and right MOctx in wt-hM3Dq mice ($p < 0.05$, TFCE corrected). We then looked for hM3Dq-induced effects in the mouse functional connectome by analysing the correlation matrices obtained from a whole-brain parcellation scheme of 130 regions (65 ROIs per hemisphere) from the Allen's Common Coordinate Framework (Dong H. W., 2008). The results confirmed that the reduction in FC in wt-hM3Dq mice following the injection of clozapine is specific to somatosensory areas (Fig. 3J, Suppl. Fig. S2C). In summary, both our hypothesis-driven and data-driven connectivity analyses demonstrate that increasing local cortical excitation by activating hM3Dq-DREADDs causes a reduction of long-range FC exclusively for the somatosensory/somatomotor networks (Fig. 3K).

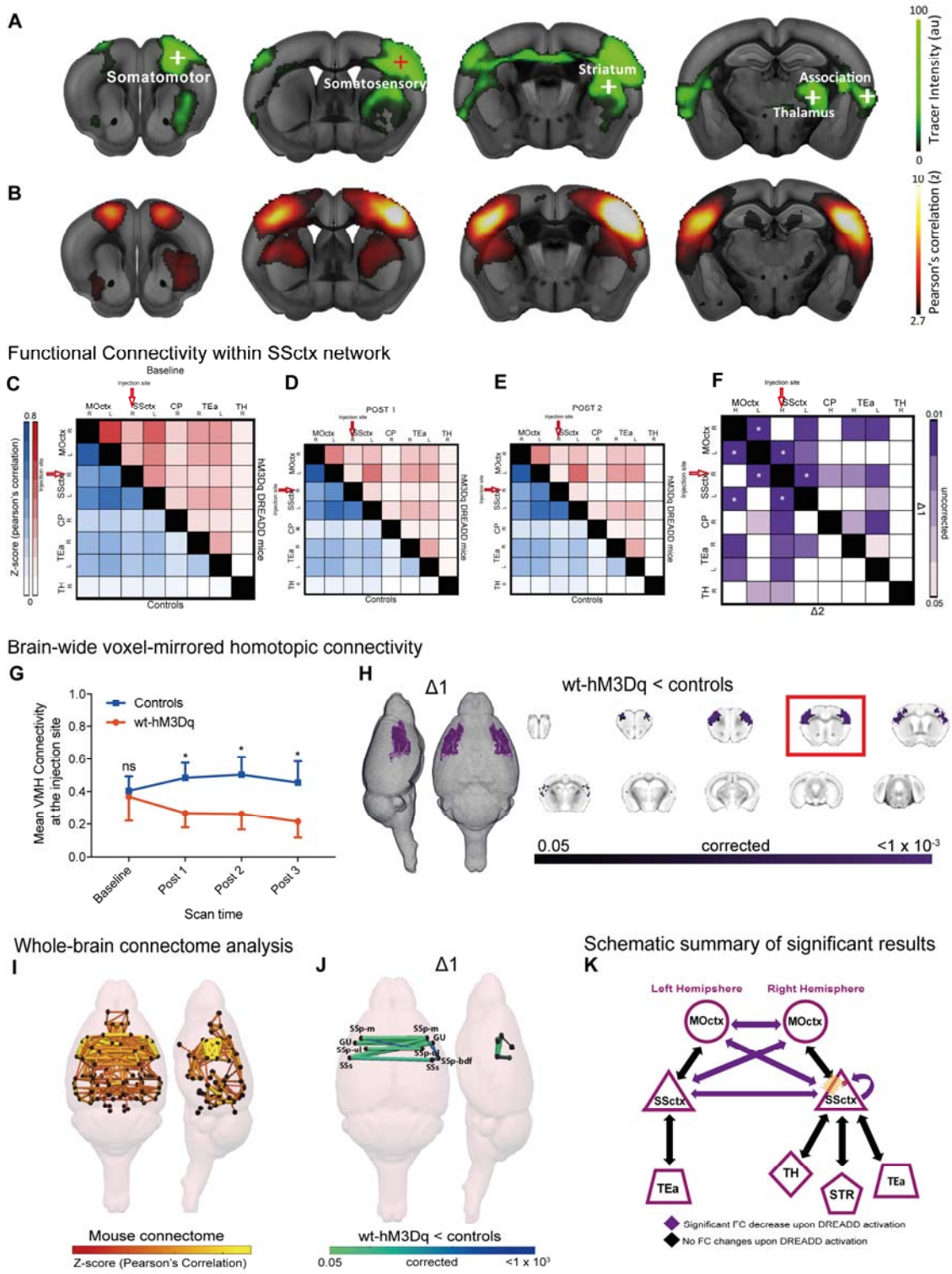

Figure 3. Long-range connectivity changes induced by activating hM3Dq. A) *Coronal brain slices depicting tracer data (green, obtained from Allen Mouse Brain Connectivity Atlas, Injection ID: 126908007).* ***B)*** *Averaged voxel-wise Pearson's correlation (Fisher's z-transform) during the baseline period from a seed in the right somatosensory cortex.* ***C) D) E)*** *Matrices represent averaged and z-transformed Pearson's correlation of all control animals (diagonally lower part of the matrix) and all wt-hM3Dq animals (diagonally upper part of*

the matrix) for baseline period, Post 1 and Post 2, respectively. ***F)*** *Matrix represents FC group comparisons among 5 brain regions (MOctx – Somatomotor cortex, SSctx – somatosensory cortex, CP –caudoputamen, TEa – temporal association cortex, and TH – thalamus, R – right, L – left). Diagonally upper half of the matrix represents reduction in FC in wt-hM3Dq mice compared to controls during Δ1, while the lower half represents these same differences but during Δ2 (randomized permutation testing, $p < 0.05$, uncorrected). The stars indicate significant differences that survived FDR correction for multiple comparisons.* ***G)*** *Change over time of the mean brain-wide VMHC (symmetric connectivity) at the injection site. Repeated measures ANOVA showed a significant interaction between the scan time and groups ($F(1.67,41.9)=21.18$; $p=0.000$).* ***H)*** *Corrected significant decrease in symmetric connectivity depicted as 3D images for Δ1, and shown through coronal slices for Δ1 time point. The slice marked with a red rectangle is the injection slice.* ***I)*** *3D Representation of mouse connectome thresholded at 5% sparsity level of connectivity weight.* ***J)*** *Whole-brain connectome analysis shows a significant interhemispheric reduction between somatosensory cortices for Δ1 time period between wt-hM3Dq mice and controls. Regions affected are as follows: SSp-m: Primary Somatosensory Area, mouth**;** GU: Gustatory areas**;** SSp-ul: Primary Somatosensory Area, upper limb**;** SSs: Supplementary somatosensory area**;** SSp-bdf: Primary Somatosensory Area, barel field; SSp-n: Primary Somatosensory Area, nose**.*** ***K)*** *Schematic summary of functional connections affected upon activation of hM3Dq DREADD. Blue arrows represent a significant decrease in functional connectivity in wt-hM3Dq mice compared to controls.*

2.5 Changing E:I balance by inhibiting GABAergic parvalbumin neurons

Changes of E:I have been proposed to underlie symptoms of many different brain disorders irrespective of whether primarily excitatory or inhibitory synapses are affected. In particular, it has been proposed that an impaired output from GABAergic PV interneurons, as observed in several mouse models for ASD, might cause reduced FC as observed in patients with similar genetic mutations (Penagarikano et al., 2011, Ajram et al., 2017, Selten et al., 2018, Wohr et al., 2015). To test this hypothesis, we studied whether reducing PV activity output in SSctx would induce short- and long-range functional hypo-connectivity. Ten Pvalb$^{tm1(cre)Arbr}$ (PVCre) mice underwent similar procedures as described above and transfected with a hM4Di-DREADD to cause hyperpolarization of the PV cells upon clozapine activation. By suppressing PV activity, we again aimed to shift the E:I balance of the somatosensory cortex towards excitation. This was confirmed by electrophysiological measurements showing an increase of average firing rate in the right SSctx up to 20% following clozapine injection (Fig. 4A-D). Strong viral expression in the right SSctx was confirmed by immunohistochemistry in PVCre-hM4Di mice (Suppl. Fig. S5).

ReHo analysis confirmed a local decrease in short-range FC in the right SSctx of PVCre-hM4Di mice (Repeated Measures ANOVA, scan time by group effect: $F(1,16)=8.29$; $p = 0.01$) compared to sham controls, which reached significance for Δ2 (post hoc paired *t*-test: $t(9)=-5.13$; $p = 0.001$. Fig. 4E). Next, we calculated changes of long-range FC within a network comprising SSctx and MOctx of both hemispheres, as identified in our previous experiment (Fig. 3G). We observed a reduction in FC between right SSctx and left MOctx after injecting clozapine in PVCre-hM4Di mice, an effect that

almost reached significance for Δ1 and Δ2 at corrected levels (randomized permutation testing, $p = 0.058$, FDR corrected; Fig. 4F). A similar trend was seen between the left and right SSctx at Δ2 (randomized permutation testing, $p = 0.06$, FDR corrected, Fig. 4F). Finally, whole-brain VMHC analysis confirmed that reducing the PV activity decreases FC between interhemispheric somatosensory and somatomotor areas (repeated measures ANOVA indicates an interaction effect of scan time by group: F(1,16)=5.935; p = 0.03; post hoc paired *t*-test showed group effect during Δ2 (p(9)=-4.6; $p = 0.001$; Fig. 4G).

In summary, our results reveal that shifting the E:I balance toward excitation by inhibiting PV interneurons led to a reduction of FC among voxels of the injection site and caused long-range hypo-connectivity, which is qualitatively similar to that observed during direct system excitation (see above). However, the size of this effect size was smaller than in wt-hM3Dq mice, possibly due to a lower number of virally transfected interneurons.

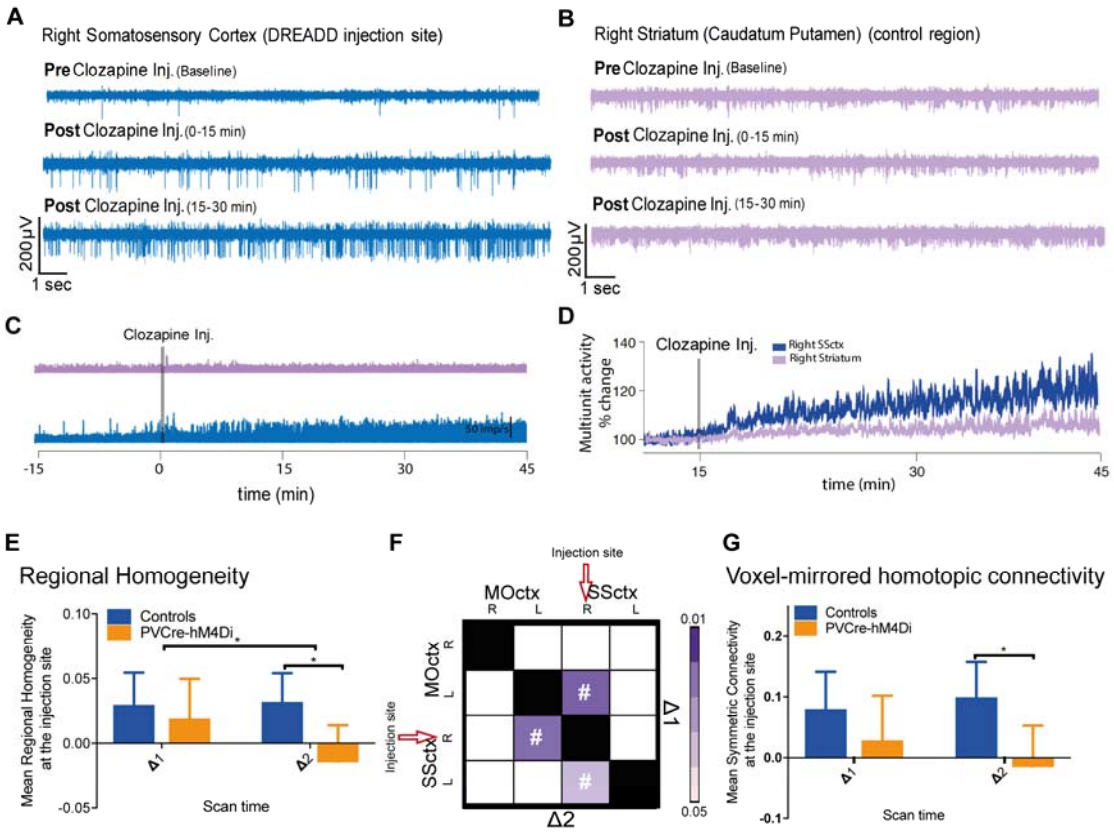

Figure 4. Changes induced by activating hM4Di in PVCre mice. A) *Figure depicts neuronal firing rate at the right somatosensory cortex (SSctx), ie. DREADD injection site, of the PVCre-hM4Di mice before and after clozapine injection, indicating a steady increase in firing rate upon DREADD activation.* ***B)*** *Similar to figure A but for right caudate putamen, indicating no change of the neuronal firing rate after clozapine injection.* ***C)*** *Time resolved firing rate in millisecond bins for the right (blue) somatosensory cortex and right striatum*

(violet). A steady increase of firing rate occurs at the right SSctx once clozapine is injected (upon 15 minutes of the baseline recording), while no change occurs at the striatum. ***D)*** *Averaged multiunit activity increased by almost 20% compared to the baseline (before clozapine injection) at the right SSctx and stayed similar to the baseline at the striatum.* ***E)*** *Normalized change over time of the mean regional homogeneity at the injection site compared between controls and PVCre-hM4Di mice. Repeated measures ANOVA showed a significant interaction between the scan time and group ($F(1,16)=8.29$; $p = 0.01$). Post hoc tests revealed a significant group difference at $\Delta 2$ ($p = 10^{-3}$) and a scan time effect ($p = 7 \times 10^{-3}$).* ***F)*** *Seed to seed analysis indicates reduced FC (randomized permutation testing, $p < 0.05$, uncorrected) between control and PVCre-hM4Di groups. MOctx – somatomotor cortex, SSctx – somatosensory cortex; R – right, L – left.* ***G)*** *Normalized change over time of the mean VMHC (symmetric connectivity) at the injection site shown for the controls and PVCre-hM4Di mice. Repeated measures ANOVA showed a significant interaction between the scan time and group ($F(1,16)=5.935$; $p = 0.03$). Post hoc paired t-test revealed a significant group difference at $\Delta 2$ ($p = 0.001$).*

2.6 Altered E:I balance changes local BOLD dynamics

We have demonstrated that increasing the E:I ratio using DREADDs changed FC, i.e. pairwise temporal correlations of rsfMRI time traces involving the injected region. Moving beyond this pairwise analysis, we next aimed at understanding how modifications in E:I balance affects the local, univariate BOLD dynamics of individual brain regions (Sethi et al., 2017, Fulcher and Jones, 2017). As depicted in Fig. 5A, we focused our analysis on three regions of interest: (i) right SSctx (the injection site); (ii) left SSctx (its homotopic counterpart); and (iii) left visual cortex (a control region). To characterize univariate BOLD dynamics, we used the software package, *hctsa* (Fulcher and Jones, 2017), which allowed us to represent each BOLD time series as a set of over 7000 features that each capture distinct properties of the dynamics (Fig. 5B) including spectral power in different frequency bands, measures of temporal entropy, and many more (Fulcher and Jones, 2017, Fulcher et al., 2013, Sethi et al., 2017) (see Methods for details). As shown in Fig. 5C, we used changes in these feature-based representations of univariate BOLD dynamics (relative to baseline) to train a linear Support Vector Machine (SVM) classifier to distinguish: (i) wt-hM3Dq versus controls, (ii) PVCre-hM4Di versus controls, and (iii) wt-hM3Dq versus PVCre-hM4Di, summarizing classification performance as the 10-fold cross-validated balanced accuracy (assigning *p*-values using permutation testing).

Here we focused our analysis on the $\Delta 1$ time period (note that qualitatively similar results were obtained at the later time period $\Delta 2$ as described in the Supplementary Results). Balanced classification accuracy of wt-hM3Dq versus control and PVCre-hM4Di versus control is plotted in Figs 5D and 5E, respectively, for each of the three brain regions. In the injected region (right SSctx), BOLD dynamics in DREADD-activated mice are significantly different from sham control mice, and can be distinguished with a balanced accuracy of 84% for wt-hM3Dq ($p = 0.001$, permutation test) and 77% for PVCre-hM4Di ($p = 0.02$). DREADD activation had a smaller effect on BOLD dynamics in the left SSctx for both wt-hM3Dq, 65% ($p = 0.1$), and PVCre-hM4Di, 64% ($p = 0.1$), and was weakest in the control region, VISctx: 43% ($p = 0.7$) in both wt-hM3Dq and PVCre-hM4Di. For the

purpose of visualizing the results, we also constructed principal components projections of each dataset (including data at Δ2), shown in Figs 5G and 5H for wt-hM3Dq versus control and PVCre-hM4Di versus control, respectively. The plots show that major features of the BOLD dynamics show little overlap between the DREADDs manipulation animals and the controls.

Since wt-hM3Dq and PVCre-hM4Di conditions increase the E:I balance through different mechanisms, we next investigated whether these two manipulations could be distinguished from each other on the basis of their univariate BOLD dynamics during Δ1. As shown in Fig. 5F, BOLD dynamics between wt-hM3Dq and PVCre-hM4Di are most distinctive in the injected region, 64% ($p = 0.12$), followed by the contralateral region, 56% ($p = 0.3$), and are least distinctive in the control region, 47% ($p = 0.6$). This trend is consistent with a characteristic difference in BOLD dynamics between wt-hM3Dq and PVCre-hM4Di, but classification rates did not deviate significantly from chance ($p > 0.1$). The lack of clear discriminability between wt-hM3Dq and PVCre-hM4Di based on BOLD dynamics is also evident in the overlapping data distributions in the principal component projections shown in Fig. 5I. To investigate this further, we quantified the similarity in how the dynamical properties of BOLD signals change in wt-hM3Dq and PVCre-hM4Di relative to sham (see Supplementary Material). Our analysis revealed a strong overall agreement in right SSctx (*rho* = 0.50) and left SSctx (*rho* = 0.44) relative to the control region. These results suggest that features of BOLD dynamics are more sensitive to the net over-excitation which is common to both DREADD cohorts, than to the underlying cellular pathway.

To interpret the univariate BOLD signature of increased E:I, we analysed the features that are individually discriminative of wt-hM3Dq, focusing on right SSctx at Δ1. A total of 924 time-series features were individually informative, revealing interpretable differences in BOLD dynamics of wt-hM3Dq relative to sham, including a decrease in signal variance and an increase in low-frequency power, as well as differences in affine scaling properties, linear and nonlinear autocorrelation, and measures of model-based predictability and entropy (see Supplementary Material for full analysis). Our results suggest that DREADDs manipulation causes characteristic changes in a wide range of interpretable dynamical properties of the BOLD signal.

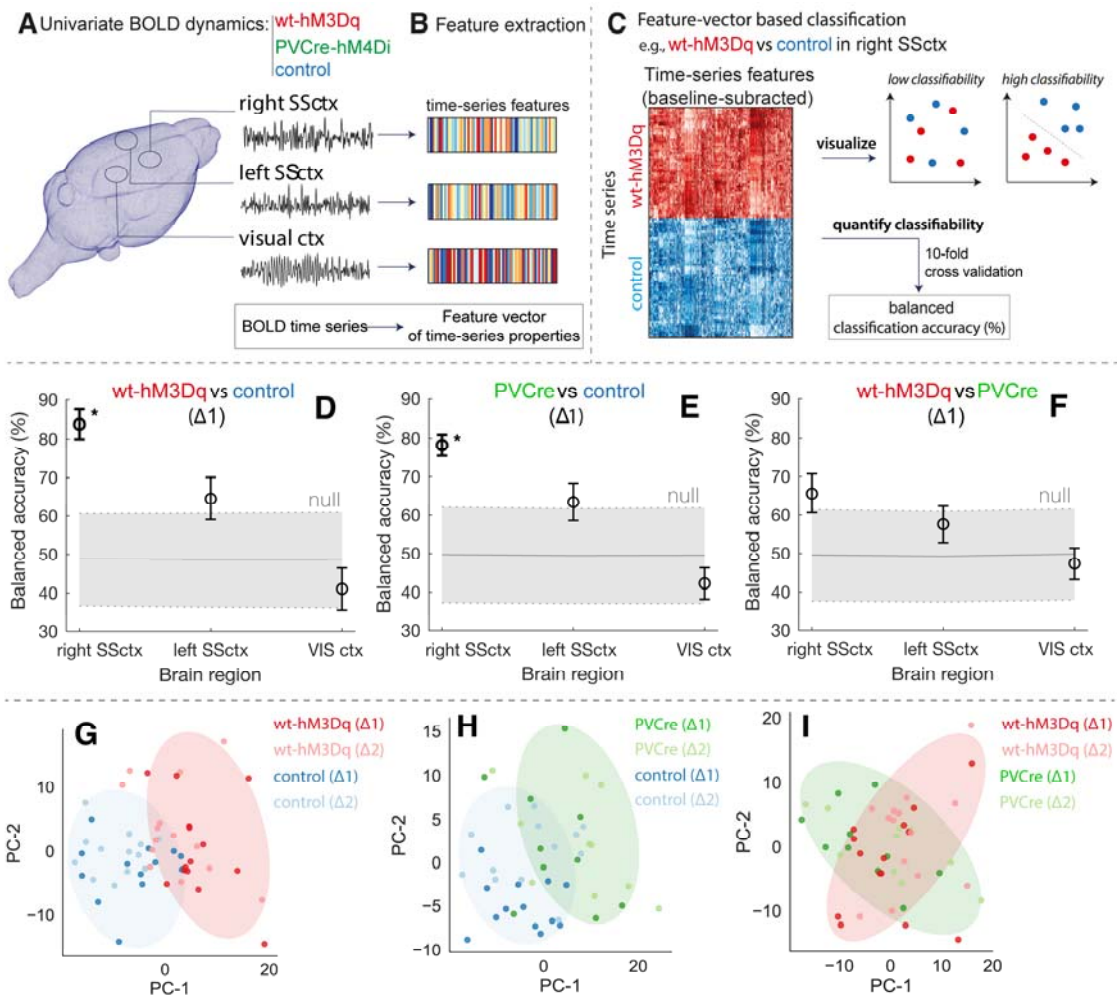

Figure 5: DREADDs lead to characteristic changes univariate BOLD dynamics in the injected region (right SSctx). *Classification of BOLD signal dynamics in three brain regions (the injected right SSctx, left SSctx, and VIS ctx) across three conditions (wt-hM3Dq, PVCre-hM4Di, and control). A schematic of approach is depicted in* ***A–C****:* ***A)*** *BOLD dynamics are measured from each brain region as a univariate time series (a 15 min time series per time window and experiment), which was* ***B)*** *converted to a set of properties (a 'feature vector') using hctsa.* ***C*** *For a given region and pair of classes, we used the features of each time series (relative to baseline) as the basis for classification, which was visualized using a low-dimensional principal components projection and quantified as the 10-fold cross-validated balanced classification accuracy (%). Classification results in each brain region at Δ1 are shown for:* ***D)*** *wt-hM3Dq versus control,* ***E)*** *PVCre-hM4Di versus control, and* ***F)*** *wt-hM3Dq versus PVCre-hM4Di, revealing significant discriminability in the right SSctx for wt-hM3Dq and PVCre-hM4Di versus control (permutation test, $p < 0.05$, annotated as* ***'*'****), and a consistent trend of high discriminability in the injected region (right SSctx), followed by the contralateral region (left SSctx), and lowest in the control region (VIS ctx). Visualizations of the time series in right SSctx are shown in two-dimensional feature spaces of leading principal components in* ***G)–I)*** *for the same three pairs of classes as in* ***D)–F).*** *Time series with similar properties are close in the space, revealing a visual depiction of the discriminability of wt-hM3Dq and PVCre-hM4Di relative to control (****G****,* ***H****), but a relative lack of discriminability for wt-hM3Dq*

*versus PVCre-hM4Di (**I**). Shaded ellipses (Δ1) have been added to guide the eye, and time series from Δ1 and Δ2 from each class are labelled.*

3. Discussion

In this proof-of-principle study, we show that long-range hypo-connectivity measured with rsfMRI, a common feature of several psychiatric conditions, can be triggered by local modulation of the E:I balance. We shifted the E:I balance towards excitation in the right SSctx area by two different mechanisms: (i) increasing net neuronal excitability of cortical circuits; and (ii) selectively inhibiting GABAergic PV neurons of the same circuits. Both manipulations caused an increase of basal firing rates, which was accompanied by a significant, anatomically-specific rise of cerebral blood flow. These changes in neural activity caused a significant reduction in FC within the injection site and between areas that share dense monosynaptic projections with the SSctx. Using machine learning to quantify discriminability of regional BOLD dynamics between conditions, we report a consistent univariate BOLD signature of a shifting E:I balance in the injected region, which was largely independent of the mechanism of the alteration, i.e. activation of excitatory circuits versus suppression of inhibitory circuits. Shifts in E:I balance might therefore represent a convergent pathway underlying divergent dynamics of macroscopic activity, which may, in turn, drive abnormal FC within large-scale brain networks, a salient feature of a range of neurodevelopmental disorders. Moreover, we provide the first direct evidence that BOLD measured at rest reflects the state of the underlying cortical microcircuits, suggesting that E:I shifts at the cellular level propagate across different temporal and spatial scales.

3.1 Activated DREADDs caused relative over-excitation at the cellular level and within cortical circuits

In our first experiment, we used hM3Dq-DREADD on human synapsin (hSyn) promoter to achieve a strong shift in E:I balance in the targeted region towards over-excitation. According to a study from Nathanson and colleagues, the hSyn promoter in AAV constructs is able to generate a clear bias towards gene expression in excitatory cortical neurons (up to 85%), which is similar to results with CAMKII of similar titer (Nathanson et al., 2009). While none of the promoters in AAV can restrict its affinity exclusively towards excitatory neurons, our electrophysiological results confirmed that activating DREADDs in the wt-hM3Dq mice caused a significant increase of neuronal firing rate in the targeted region, suggesting a general over-excitation. Convergent evidence is also revealed by our CBF measurements. CBF is reflective of glucose metabolism as indicated by numerous PET and fMRI studies and is considered an indirect marker of neural activity at the populations level (Chen et al, 2008; Schlegel et al., 2018; Jueptner and Weiller, 1995). Here we report an increase of CBF exclusively in the right SSctx of the DREADD mice, which confirms (i) the increased excitation of the targeted area and (ii) the anatomical specificity of our intervention.

In the second series of experiments we used PVCre mice ensuring cell-specificity of the hM4Di DREADDs. Analogous to our first experiment, in vivo electrophysiology confirmed that inhibiting GABAergic PV neurons via hM4Di DREADDs significantly increased neuronal population firing. This agrees with previous literature, which states that suppression of PV interneurons leads to an increased cortical excitation i.e. increase in number of cells spiking at the population level (Moore et al., 2018, Selimbeyoglu et al., 2017, Wilson et al., 2012, Atallah et al., 2012). In summary, even though the two experiments targeted different biological pathways, both manipulations converged in shifting the cortical E:I balance caused by a net increase of firing of neuronal populations within the targeted SSctx, as shown by convergent evidence from in vivo electrophysiology and cerebral blood flow.

In order to activate DREADDs, we used low-doses of clozapine instead of the most commonly used clozapine-N-oxide (CNO). Clozapine is a potent antipsychotic medication used in treatment of schizophrenia and binds to a number of receptors including serotonin, α1-adrenergic receptors, muscarinic-1, histamine (Nucifora et al., 2017). Clozapine is a metabolite of CNO but, unlike CNO, is able to freely pass the blood brain barrier. Because of its high affinity for DREADD receptors, clozapine is thought to be the actual actuator of DREADDs in *in-vivo* studies (Gomez et al., 2017, Manvich et al., 2018). In our experiments, we used clozapine doses of 0.03-0.01 mg/Kg to activate the DREADD, which are below the threshold level necessary to elicit a behavioral effect in mice. To further control for any unspecific effect of clozapine, we employed a cross-sectional design, injecting identical doses of clozapine in sham-operated mice as controls. We also conducted experiments using two different doses of clozapine (Suppl. Fig. S6) and found no differences in the effects of clozapine in any of the groups, suggesting that the lower dose (0.01mg/kg) is sufficient to activate DREADDs *in vivo*. On top of that, we performed analogous experiments in smaller mouse cohorts using CNO, which revealed similar effects i.e. a significant decrease in interhemispheric connectivity at the somatomotor cortex (Suppl. Fig. S3).

3.2 Activated excitatory DREADD in wildtype mice and inhibitory DREADD in PVCre mice both induce connectivity reduction

Reduced FC is an observation often reported in human fMRI studies of neurodevelopmental disorders, such as autism and schizophrenia (Gao and Penzes, 2016, Uhlhaas and Singer, 2006) (Kraguljac et al., 2016, Sforazzini et al., 2016, Cherkassky et al., 2006, Just et al., 2007, Minshew and Keller, 2010, Gur and Gur, 2010, Wang et al., 2018), as well as in t relevant mouse models of these disorders (Liska et al., 2018, Zerbi et al., 2018b). One of the prevailing hypotheses is that lack of sufficient PV interneuron expression is causative for the observed aberrant patterns of neural activity and connectivity (Wohr et al., 2015, Penagarikano et al., 2011). Fast spiking PV interneurons target the proximal regions of pyramidal cells (Hu et al., 2014, Safari et al., 2017) and have been suggested

to play an important role in regulating the precise timing of pyramidal cell spikes, thus coordinating their synchrony through gamma oscillations (Cardin, 2018, Sohal et al., 2009, Cardin et al., 2009, Bartos et al., 2007, Fries et al., 2001, Engel and Singer, 2001, Roux and Buzsaki, 2015). Sensory-evoked gamma oscillations from cortical in vivo recordings and synchronized, phase-locked firing of pyramidal cells, indicate entrainment of excitatory neurons to rhythmic inhibitory activity (Fries et al., 2001, Hasenstaub et al., 2005, Cardin et al., 2009, Gray et al., 1989). Because gamma oscillations are thought to control the synchronization of pyramidal cells (Marissal et al., 2018, Cardin, 2018, Buzsaki and Wang, 2012, Cardin et al., 2009), a reduced PV activity would result in a lack of generated gamma oscillations (Roux and Buzsaki, 2015), which in turn gives rise to asynchronous firing of pyramidal cells. This hypothesis has been recently confirmed by Marissal and colleagues, which found that DREADD-induced suppression of PV activity results in reduced inhibition of pyramidal neurons and leads to their mass desynchronization (Marissal et al., 2018). Moreover, they showed that increasing the inhibition of pyramidal neurons in wildtype mice, thus shifting the E:I towards inhibition, has no effect on neural synchronization, in-vitro network dynamics or behaviour. In line with these previous findings we suggest that the reduction of local and long-range FC observed in our experiments is likely to reflects reduced *synchronization* of neuronal mass activity despite higher net cortical activity within the targeted SSctx. Note that unlike certain optogenetic tools, DREADDs influence neural activity through endogenous signalling mechanisms which modulate a cell's input control by up-weighting or down-weighting excitability without artificially imposing a temporally specific firing pattern across large neuronal ensembles (Alexander et al., 2009). DREADDs-induced changes were specific to the injection area and to anatomically connected regions and observed over and above variations of functional connectivity as measured in control mice which underwent the exact same rsfMRI procedures. The reduction in FC was generally stronger in the wt-hM3Dq mice than in the PVCre-hM4Di mice, which could be linked to a difference in number of transfected neurons between the two groups. Mouse cortex contains 12% GABAergic neurons, of which approximately one quarter are PV (Feldmeyer et al., 2018, Packer and Yuste, 2011). Thus, the smaller effect size observed in our PVCre-hM4Di mice could be explained by the lower number of virally transfected neurons, an effect already reported in monkeys by rsfMRI (Grayson et al., 2016).

3.3 BOLD timeseries dynamics as a mediator of reductions in functional connectivity

Moving beyond previous analyses of rsfMRI that largely focused on quantifying measures of pairwise temporal correlations between BOLD time series (i.e. FC), we also investigated the dynamic properties of BOLD fluctuations in individual brain regions, allowing us to obtain a better understanding of the effect of DREADDs on local BOLD dynamics. Increasing the E:I ratio through DREADDs activation caused characteristic changes in BOLD dynamics in the injected region (right SSctx) relative to controls, allowing individual BOLD time series to be classified as response to DREADD activation or sham treatment with high accuracy. Activation of both DREADDs, wt-hM3Dq and PVcre-hM4Di, caused similar changes in BOLD dynamics in the injected area. This

suggests that the observed effects results from the increased E:I ratio irrespective of which neurobiological pathways causes the excitation increase at the circuit level (i.e. whether it be an increase in net neuronal activation or release of inhibition).

4. Conclusions

In conclusion, here we provide the first causal evidence that an increase in net cortical excitation can alter the BOLD dynamics signature such that local and long-range functional connectivity are reduced at the macroscopic level. Even though two different biological pathways were used to perturb the neural dynamics within cortical microcircuits (i.e. excitation versus release of inhibition), the macroscopic effects were highly similar. This suggests that an increase of the E:I ratio represents a convergent mechanism which underpins long-range hypo-connectivity, a phenomenon frequently observed in neurodevelopmental disorders. Our results demonstrate the value of a DREADD-fMRI approach for identifying the causal link between neural activity at the cell population level and markers of brain-wide, macroscopic functional connectivity as measured with rsfMRI in mice. Understanding the neurobiology underlying abnormal BOLD dynamics and long-range functional connectivity measured with rsfMRI is an important first step towards establishing rsfMRI as a translational and a clinical tool.

5. Acknowledgment

We thank the team of the EPIC animal facility for providing animal care. We thank Jean-Charles Paterna from the Viral Vector Facility (VVF) of the Neuroscience Center Zurich, a joint competence center of ETH Zurich and University of Zurich for producing viral vectors and viral vector plasmids. We thank Amalia Floriou Servou and Mattia Privitera for useful feedback regarding immunohistochemistry.

6. Financial Support

This project is supported by the ETH Research Grant ETH-38 16-2. VZ is supported by ETH Career Seed Grant SEED-42 54 16-1 and by the SNSF AMBIZIONE PZ00P3_173984/1.

7. Experimental Procedures

All experiments and procedures were conducted following the Swiss federal Ordinance for animal experimentation and approved by Zurich cantonal Veterinary Office (ZH238/15). C57BL/6 mice were obtained from Charles River Laboratories (Germany), while Pvalb$^{tm1(cre)Arbr}$ (PVCre) mice were derived from in-house breeding (first generation obtained from the Jackson Laboratory). All mice were kept in standard housing under 12h light/dark cycle with food and water provided *ad libitum* throughout the whole experiment. A total of 18 male C57BL/6 mice were used in the experiment, aged 15 ± 2 weeks and weighing 24.3 ± 2.3gr (mean ± SD) at the day of the surgery. A total of 10 PVCre mice were utilized in this experiment, aged 21 ± 1 weeks and weighing 26.1± 3.8gr at the day of the surgery.

7.1.1 Procedures for wildtype (hM3Dq) mice study

7.1.1 Transfection procedures for wildtype (wt-hM3Dq) mice

Each mouse was initially anesthetized using a mixture of midazolam (5mg/ml; Sintetica, Switzerland), fentanyl (50mcg/ml; Actavis AG, Switzerland) and medetomidine (1mg/ml; Orion Pharma, Finland). Upon anesthesia induction, mice were placed on a heating pad and the temperature was kept at 35ºC (Harvard Apparatus, USA). Following shaving and cleaning, an incision along the midline of scalp was made. The right primary somatosensory cortex was targeted at the coordinates of +0.5 mm AP (anterior-posterior), -3.0 mm ML (medio-lateral) and -2.25 mm DV (dorso-ventral) relative to Bregma using a drill and microinjection robot (Neurostar, Germany) with a 10 ul NanoFil syringe and 34Ga bevelled needle (World Precision Instruments, Germany). 950 nl of ssAAV8-hSyn-hM3Dq-mCherry (n=13) of a physical titer $\geq$ 5.4 x 10^{12} vg/ml (*vector genomes; fluorometric quantification) was injected at the rate of 0.06 ul/min. The virus was provided by Viral Vector Core Facility of the Neuroscience Centre Zurich (http://www.vvf.uzh.ch/en.html). Upon the injection, the needle was left in place for 10 min and then slowly withdrawn. C57BL/6 control mice (n=9) underwent the same surgical procedures, where the needle was kept in place for 5min but without any viral injections. Subsequently, mice were given an anesthesia antidote consisting of tegmestic (0.3mg/ml; Reckitt Benckiser AG, Switzerland), annexate (0.1mg/ml; Swissmedic, Switzerland) and antisedan (0.1mg/ml; Orion Pharma, Finland) and left to fully recover. Following the surgery, ketoprofen (10mg/kg; Richter Pharma AG, Austria) was subcutaneously injected daily for at least 3 days to reduce any post-operative pain. Animals were given 3-4 weeks to fully recover from the surgery and to allow for expression of the transgene prior to the scanning session.

7.1.2 Electrophysiological recordings

The electrophysiological data used for verification of neuronal activity were acquired in 4 wt-hM3Dq animals. Briefly, animals were anesthetized with isoflurane to match conditions used in imaging studies (2-4% for induction, 0.5% for data collection), and their body temperature was maintained using a heating pad. A small craniotomy was performed over the right and left somatosensory cortex

and the brain was covered with silicone oil. A small trepanation was performed over the cerebellum and a silver wire was placed in contact with the CSF to serve as reference electrode. For hM3Dq validation, one silicon probe (Atlas Neurotechnologies, 16 sites, 100 µm spacing) was implanted in each hemisphere. After implantation, we waited 20-30 minutes in order to allow the recording to stabilize. After stabilization, the broadband voltage was amplified and digitally sampled at a rate of 30kHz or 48kHz using one of two commercial extracellular recording systems (Intan or Axona). The raw voltage traces were filtered off-line in order to separate the multi-unit activity (bandpass filter 0.46-6 kHz) using a second order Butterworth filter. Subsequently, the highpass data were thresholded at 4.5 times the standard deviation across the recording session and the number of spikes in 10 second windows were counted. Recording sessions lasted for 45 minutes. At 15 minutes following the start of the recordings (baseline) 30 µg/kg clozapine was injected (intravenously). In order to combine data across mice, the activity at sites with clear multi-unit activity was expressed in percent of the baseline value, i.e. each 10s bin of MUA activity was divided by the average spike rate during the 15 minute pre-injection baseline (100%). All multi-units were then combined from the injected or control region.

7.1.3 MRI setup and Animal preparation

Two MRI sessions were performed on a 7T Bruker BioSpec scanner equipped with a Pharmascan magnet, with two coil setups optimized for the two different acquisition sequences i.e. Arterial Spin Labeling (ASL) and resting-state fMRI (rsfMRI). First, the ASL was obtained utilizing a receiver-only surface coil, coupled with a volume resonator for radiofrequency (rf) transmission. For rsfMRI measurements, a high signal-to-noise ratio (SNR) receive-only cryogenic coil (Bruker BioSpin AG, Fällanden, Switzerland) was used in combination with a linearly polarized room temperature volume resonator for rf transmission.

Standardized anesthesia protocols and animal monitoring procedures were utilized for both MRI sessions (Zerbi et al., 2018b). Briefly, mice were initially anesthetized with 4% isoflurane in 1:4 O_2 to air mixture for 4 min to allow for endotracheal intubation and tail vein cannulation. Mice were positioned on an MRI-compatible support, equipped with hot water-flowing bed to keep the temperature of the animal constant throughout the entire measurement (36.6 ± 0.5 ºC). The animals were fixed with ear bars and mechanically ventilated via a small animal ventilator (CWE, Ardmore, USA) at the rate of 80 breaths per minute, with 1.8 ml/min flow with isoflurane at 2%. Subsequently, a bolus containing a mixture of medetomidine (0.05mg/kg) and pancronium (0.25mg/kg) was injected via the cannulated vein and isoflurane lowered at 1%. Five minutes following the bolus injection, a continuous infusion of medetomidine (0.1mg/kg/h) and pancronium (0.25mg/kg/h) was started while isoflurane was further reduced to 0.5%. Animal preparation took on average 15.5 ± 2.7 minutes and all animals fully recovered within 10 minutes after the measurement.

7.1.4 Arterial Spin Labeling (ASL)

Brain perfusion was measured using an established arterial spin labelling (ASL) method using a flow sensitive alternating inversion recovery (FAIR) sequence (Zerbi et al., 2014). Briefly, a two-segment

Spin-Echo was used with following parameters: echo time TE=12.47 ms, recovery time TR=13000 ms, image matrix=128 x 96, field of view=20 x 20 mm, slice thickness= 1 mm, spatial resolution = 0.156 x 0.208 x 1 mm/pixel. Inversion parameters: inversion time = 40 ms, inversion slab thickness = 4 mm, slice margin = 1.5 mm. Sixteen images at different inversion times (100ms to 3s) were obtained for T_1 calculations, resulting in a scan time of 15 minutes (referred to as baseline). After the first baseline acquisition, clozapine was intravenously injected at 10-30 µg/kg and three more sessions were acquired (i.e. Post 1, Post 2 and Post 3, respectively), resulting in a total scan time of one hour. A total of 13 animals (5 controls and 8 wt-hM3Dq mice) were scanned.

Data Analysis

$T_{1selective}$ and $T_{1nonselective}$ were determined by fitting the signal intensities in each voxel with 3-parameters monoexponential T_1 relaxation curve. The perfusion was calculated according to:

$$\frac{CBF}{\lambda} = \frac{T1_{nonselective}}{T1_{blood}}\left(\frac{1}{T1_{selective}} - \frac{1}{T1_{nonselective}}\right)$$

where λ is the blood/tissue partition coefficient, assumed to be 0.9ml/g (Leithner et al., 2008) and T_{1blood} value at 7T of 2.25s. Perfusion was evaluated in three regions of interest: right somatosensory cortex (i.e. injection site), left somatosensory cortex (contralateral to the injection site), and right lateral striatum. Custom-written algorithms were implemented in MATLAB R2015b (Mathworks, Natick, MA, USA) to perform these calculations.

7.1.5. Resting-state fMRI (rsfMRI)

Acquisition parameters were following: repetition time TR=1s, echo time TE=15ms, flip angle= 60°, matrix size = 90x50, in-plane resolution = 0.2x0.2mm^2, number of slices = 20, slice thickness = 0.4mm, 3600 volumes for a total scan of 60 minutes. Clozapine was intravenously injected 15 min after the scan start at the doses of 10 µg/kg or 30 µg/kg. A total of 27 C57BL/6 animals (13 controls and 14 wt-hM3Dq mice) were scanned. These include 8 C57BL/6 animals that were scanned twice (4 controls and 4 wt-hM3Dq mice), once with 10 µg/kg dose of clozapine and another with a 30 µg/kg dose of clozapine (suppl. Table 1).

Data Analysis

Data was preprocessed using an already established pipeline for removal of artefacts from the time-series (Zerbi et al., 2015, Sethi et al., 2017). Briefly, each 4D dataset was normalized in a study-specific EPI template (Advanced Normalization Tools, ANTs v2.1, picsl.upenn.edu/ANTS) and fed into MELODIC (Multivariate Exploratory Linear Optimized Decomposition of Independent Components) to perform within subject special-ICA with a fixed dimensionality estimation (number of components set to 60). The procedure included motion correction and in-plane smoothing with a 0.3 mm kernel. FSL-FIX study-specific classifier, obtained from an independent dataset of 15 mice,

was used to perform a 'conservative' removal of the variance of the artefactual components (Griffanti et al., 2014). Subsequently, the dataset was despiked (Patel et al., 2014), band-pass filtered (0.01-0.25 Hz) and finally normalized into AMBMC template (www.imaging.org.au /AMBMC) using ANTs. Each dataset was split into four parts of 900 data points (equivalent of 15 minutes of scanning). The difference between the baseline (first 15 minutes of scan) and the rest of the bins are further referred to as Δ1, Δ2 and Δ3.

Seed to seed analysis

The "somatosensory network" in the mouse was defined anatomically using the tracer-based axonal projection pattern of SSctx from the Allen Mouse Brain Connectivity atlas (experiment no. 126908007) and contained contralateral primary SSctx, bilateral somatomotor cortex (MOctx), bilateral association cortices (TEa), as well as ipsilateral caudoputamen (CP) and thalamus (TH (Parafascicular nucleus))(Oh et al., 2014) (Grandjean et al., 2017). BOLD time series from these regions were extracted using a voxel cube of 3mm. Full correlation Z-scored matrices were calculated using FSLNets (FMRIB Analysis Group).

Regional Homogeneity (ReHo)

Voxel-wise Regional Homogeneity (ReHo) maps were computed using AFNI (Cox W. R., 1996). ReHo was calculated for a given voxel and its 19 nearest neighbours and smoothened by Gaussian kernel with Full Width of Half Maximum (FWHM) equal to 10.

Voxel-mirrored homotopic connectivity (VMHC)

VMHC measures the similarity between any pair of symmetric inter-hemispheric voxels by computing the Pearson's correlation coefficient between the time series of each voxel and that of its exact symmetrical inter-hemispheric counterpart. VMHC was computed for all the four timeseries bins and normalized to the baseline for each mouse.

Functional connectome analysis

Whole-brain correlation matrices were obtained from a parcellation scheme of 130 regions using the Allen Mouse Brain ontology (Oh et al., 2014). In total, 65 regions of interest (ROIs) per hemisphere were considered, including regions from isocortex, hippocampal formation, cortical subplate, striato-pallidum, thalamus, midbrain and hindbrain.

Statistical analysis

Prior to performing statistical tests, within-subject normalization to the baseline was implemented. FSL General Linear Model (GLM) was used to perform statistical comparison between controls and wt-hM3Dq mice for the rs-fMRI data (including seed to seed analysis, ReHo, VMHC, connectome analysis). We performed nonparametric permutation testing with 5000 permutations, using family-wise error correction with threshold-free cluster enhancement (TFCE). Statistical significance was defined as $p < 0.05$. CBF differences were statistically tested using linear mixed models implemented in SPSS24 (IBM, USA). All the statistical analysis included 6 covariates: (i) mouse age at the time of surgery; (ii) bodyweight at the time of the scan; (iii) total scan preparation time ie. time between the

first anaesthesia induction to the start of the resting-state scan; (iv) bolus time ie. time from the first anaesthesia induction to the start of the continuous anaesthetic infusion (isoflurane at 0.5%); (v) the number of ICA components rejected using FSL-FIX and (vi) clozapine dose. These covariates were implemented in all the statistical tests for all types of analysis performed.

7.2 Procedures for PVCre (hM4Di) mice study

7.2.1. Transfection procedures for PVCre-hM4Di mice

The right primary somatosensory cortex of PVCre mice (mice expressing Cre recombinase in parvalbumin-expressing neurons) was unilaterally targeted with 950nl of ssAAV8-hSyn1-dlox-hM4Di_mCherry(rev)-dlox-WPRE-hGHp(A) (n=10) of a physical titer $\geq 5.4 \times 10^{12}$ vg/ml (*vector genomes; fluorometric quantification) at the rate of 0.06 ul/min. The same procedures for animal preparation, anaesthesia and coordinates were used as already described for wildtype mice in section 2.1.1.

7.2.2. In vivo electrophysiology

Four PVCre-hM4Di mice underwent in vivo electrophysiological recordings following the same procedures as described for wildtype mice (Section 2.1.2). The only difference was in the location of the control probe (Atlas Neurotechnologies, 32 sites, 100 µm spacing), which was implanted into the right (ipsilateral to the DREADD injection site) striatum.

7.2.3 RsfMRI acquisition

Preparation and anaesthesia used for the scanning of the PVCre-hM4Di mice was identical to the procedures outlined for wildtype mice (Section 2.1.3). The two acquisitions only differed in the length of the scan. The PVCre-hM4Di mice were scanned for 45 minutes where clozapine was intravenously injected at 15 minutes at the dose of 30mg/ml.

7.2.4. RsfMRI analysis

Data were acquired using matching sequence to the wildtype mice, and the preprocessing was performed following the same pipeline described in Section 2.1.5.

Seed-to-seed analysis

Based on the results obtained from wt-hM3Dq mice, BOLD timeseries was extracted bilaterally from somatomotor and somatosensory cortices (resulting in 4 seeds) using a voxel cube of 3mm. Full correlation *z*-scored matrices were calculated and statistically compared.

7.3 Feature extraction and classification of univariate BOLD time series

7.3.1. Data processing and computation

We analysed the properties of univariate BOLD time series measured from three brain regions: (i) right SSctx (injected region), (ii) left SSctx (contralateral region), and (iii) visual cortex (control region). One-hour long time series measurement was split into four 15-minute time points in three

classes of experiment: (i) wt-hM3Dq (14 mice), (ii) PVCre-hM4Di (10 mice), and (iii) sham controls (13 mice). To understand which time-series properties distinguish different experimental conditions, we converted each univariate time series to a vector of 7873 interpretable properties (or features) using *v0.9.6* of the *hctsa* toolbox (Fulcher and Jones, 2017, Fulcher et al., 2013). Time-series data measured in each brain region could then be represented as a 108 (experiments) × 7873 (time-series features) data matrix. Features that had well-behaved outputs across the whole dataset and were non-constant within all the three groups were retained for further analysis (7279 features). Each time series was labelled by its experimental condition ('wt-hM3Dq', 'PVCre-hM4Di', or 'sham') and time-point ('baseline', 't2', and 't3').

7.3.2. Classification

We used the feature-based representations of BOLD time-series in each brain area as the basis for machine-learning classification of the different experimental conditions. We focused our analysis on the Δ1 time period, first subtracting time-series features computed at baseline, and then normalizing these feature differences using an outlier-robust sigmoidal transformation (Fulcher et al., 2013). A linear support vector machine classification model was learned on the normalized feature matrix for a given brain area. A measure of discriminability of a pair of classes was quantified as the balanced classification accuracy using 10-fold stratified cross validation (balanced accuracy was computed as the arithmetic mean of sensitivity and specificity to account for the small class imbalance: 13 sham controls and 14 wt-hM3Dq or 10 PVCre-hM4Di mice). To reduce variance in the random partition of data into 10 folds, we repeated this procedure 50 times (with each iteration yielding a balanced accuracy value). This distribution was summarized as its mean and standard deviation.

In smaller samples, the possibility that optimistic classification results could be obtained by chance is heightened. To quantify this, here we evaluated the statistical significance of our classification results relative to random assignments of class labels to data. We achieved this by computing a null distribution of the same performance metric used above (mean across 50 repeats of 10-fold cross-validated balanced accuracy) for 5000 random class label assignments to time series. The statistical significance of a given classification result was then estimated as a permutation test (as the proportion of 5000 null samples with a mean balanced classification rate exceeding that of the true assignment of class labels). Differences in 10-fold balanced classification accuracy between brain regions were assessed using Welch's *t*-tests (as each accuracy distribution was approximately normally-distributed).

7.3.3. Low-dimensional projections

Using *hctsa*, BOLD time series are converted into large feature vectors, such that each time series can be considered as a point in this high-dimensional feature space. To aid visualization of the class structure of data in this space, we can projected normalized time series × feature data matrices into a lower-dimensional space that captures the maximal variance in the full feature space using principal

components analysis. In these plots, individual time series are points in the space, providing an intuitive visualization of dataset structure.

7.3.4. Interpreting differences in univariate dynamics

We aimed to determine which properties of the univariate BOLD dynamics in the injected brain area best discriminated wt-hM3Dq from sham controls, PVCre-hM4Di from controls and wt-hM3Dq from PVCre-hM4Di mice. Focusing on the first time period after baseline, we first computed the difference in each feature value between this first time period and the baseline period ($\Delta 1$). We then tested whether these relative feature values differed between groups using a Wilcoxon rank-sum test. We corrected for the large number of hypothesis tests using the false discovery rate (Benjamini and Hochberg, 1995), setting a significance threshold of $q = 0.05$.

7.4 Histological evaluation of transfection

DREADDs viral expression (for both wt-hM3Dq and PVCre-hM4Di) was confirmed by m-Cherry staining using standard immunohistochemistry protocols (Notter et al., 2014, Floriou-Servou et al., 2018). Briefly, after the last MRI session mice were deeply anesthetized using a mixture of Ketamine (100mg/kg; Graeub, Switzerland), Xylazine (10mg/kg; Rompun, Bayer) and Acepromazine (2mg/kg; Fatro S.p.A, Italy) and transcardially perfused with 4% Paraformaldehyde (PFA, pH=7.4). The brains were postfixed in 4% PFA for 1.5 hours at 4°C and then placed overnight in 30% sucrose solution. Brains were frozen in a tissue mounting fluid (Tissue-Tek O.C.T Compund, Sakura Finetek Europe B.V., Netherlands) and sectioned coronally in 40 μm thick slices using a cryostat (MICROM HM 560, histocom AG-Switzeland). Free-floating slices were first permeabilized in 0.2% Triton X-100 for 30 min and then incubated overnight in 0.2% Triton X-100, 2% normal goat serum and rabbit anti-mCherry (1:1000, Ab167453, Abcam) at 4ºC under continuous agitation (100rpm/min). The next day sections were incubated for 1h in 0.2% Triton X-100, 2% normal goat serum, goat anti-rabbit Alexa Flour 546 (1:300, A11035, Life Technologies) and Nissl (1:300, NeuroTrace 660, Thermo Molecular Probes) or DAPI (1:300, Sigma-Aldrich) at room temperature under continuous agitation. Afterwards, slices were mounted on the superfrost slides where they were left to airdry and later coverslipped with Dako Flourescence mounting medium (Agilent Technologies). Confocal laser-scanning microscope (Leica, SP8, Centre for Microscopy and Image Analysis, UZH) and Zeiss Slidescanner (Zeiss Axio scan, Z1, Centre for Microscopy and Image Analysis, UZH) were used to detect the viral expression. Microscopy protocol included a tile scan with a 10x or a 20x objective, pixel size of 1.2μm and image size of 1024x1024 pixels. Images were preprocessed and analyzed using ImageJ-Fiji and Zeiss Zen Blue, respectively.

8. References

Ajram, L. A., Horder, J., Mendez, M. A., Galanopoulos, A., Brennan, L. P., Wichers, R. H., Robertson, D. M., Murphy, C. M., Zinkstok, J., Ivin, G., Heasman, M., Meek, D., Tricklebank, M. D., Barker, G. J., Lythgoe, D. J., Edden, R. a. E., Williams, S. C., Murphy, D. G. M. & Mcalonan, G. M. 2017. Shifting brain inhibitory balance and connectivity of the prefrontal cortex of adults with autism spectrum disorder. *Transl Psychiatry,* 7**,** e1137.

Alaerts, K., Woolley, D. G., Steyaert, J., Di Martino, A., Swinnen, S. P. & Wenderoth, N. 2014. Underconnectivity of the superior temporal sulcus predicts emotion recognition deficits in autism. *Soc Cogn Affect Neurosci,* 9**,** 1589-600.

Alexander, G. M., Rogan, S. C., Abbas, A. I., Armbruster, B. N., Pei, Y., Allen, J. A., Nonneman, R. J., Hartmann, J., Moy, S. S., Nicolelis, M. A., Mcnamara, J. O. & Roth, B. L. 2009. Remote control of neuronal activity in transgenic mice expressing evolved G protein-coupled receptors. *Neuron,* 63**,** 27-39.

Atallah, B. V., Bruns, W., Carandini, M. & Scanziani, M. 2012. Parvalbumin-expressing interneurons linearly transform cortical responses to visual stimuli. *Neuron,* 73**,** 159-70.

Balsters, J. H., Mantini, D. & Wenderoth, N. 2017. Connectivity-based parcellation reveals distinct cortico-striatal connectivity fingerprints in Autism Spectrum Disorder. *Neuroimage*.

Bartos, M., Vida, I. & Jonas, P. 2007. Synaptic mechanisms of synchronized gamma oscillations in inhibitory interneuron networks. *Nat Rev Neurosci,* 8**,** 45-56.

Benjamini, Y. & Hochberg, Y. 1995. Controlling the False Discovery Rate: A Practical and Powerful Apporach to Multile Testing. *Journal of Royal Statistical Society: Series B (Methodological),* 57(1)**,** 289-300.

Bertero, A., Liska, A., Pagani, M., Parolisi, R., Masferrer, M. E., Gritti, M., Pedrazzoli, M., Galbusera, A., Sarica, A., Cerasa, A., Buffelli, A., Tonini, R., Buffo, A., Gross, C., Pasqualetti, M. & Gozzi, A. 2018. Autism-associated 16p11.2 microdeletion impairs prefrontal functional connectivity in mouse and human. *Brain,* 141**,** 2055-2065.

Buzsaki, G. & Wang, X. J. 2012. Mechanisms of gamma oscillations. *Annu Rev Neurosci,* 35**,** 203-25.

Cardin, J. A. 2018. Inhibitory Interneurons Regulate Temporal Precision and Correlations in Cortical Circuits. *Trends Neurosci,* 41**,** 689-700.

Cardin, J. A., Carlen, M., Meletis, K., Knoblich, U., Zhang, F., Deisseroth, K., Tsai, L. H. & Moore, C. I. 2009. Driving fast-spiking cells induces gamma rhythm and controls sensory responses. *Nature,* 459**,** 663-7.

Cherkassky, V. L., Kana, R. K., Keller, T. A. & Just, M. A. 2006. Functional connectivity in a baseline resting-state network in autism. *Brain Imaging,* 16.

Cox W. R. 1996. AFNI: Software for Analysis and Visualization of Functional Magnetic Resonance Neuroimages. *Computers and Biomedical Research,* 162-173.

Di Martino, A., Yan, C. G., Li, Q., Denio, E., Castellanos, F. X., Alaerts, K., Anderson, J. S., Assaf, M., Bookheimer, S. Y., Dapretto, M., Deen, B., Delmonte, S., Dinstein, I., Ertl-Wagner, B., Fair, D. A., Gallagher, L., Kennedy, D. P., Keown, C. L., Keysers, C., Lainhart, J. E., Lord, C., Luna, B., Menon, V., Minshew, N. J., Monk, C. S., Mueller, S., Muller, R. A., Nebel, M. B., Nigg, J. T., O'hearn, K., Pelphrey, K. A., Peltier, S. J., Rudie, J. D., Sunaert, S., Thioux, M., Tyszka, J. M., Uddin, L. Q., Verhoeven, J. S., Wenderoth, N., Wiggins, J. L., Mostofsky, S. H. & Milham, M. P. 2014. The autism brain imaging data exchange: towards a large-scale evaluation of the intrinsic brain architecture in autism. *Mol Psychiatry,* 19**,** 659-67.

Dong H. W. 2008. The Allen Reference Atlas: A digital color brain atlas of the C57Bl/6J male mouse. *Hoboken, NJ US: John Wiley & Sons Inc*.

Engel, A. K. & Singer, W. 2001. Temporal binding and the neural correlates of sensory awareness. *TRENDS in Cognitive Sciences,* 5.

Feldmeyer, D., Qi, G., Emmenegger, V. & Staiger, J. F. 2018. Inhibitory interneurons and their circuit motifs in the many layers of the barrel cortex. *Neuroscience,* 368**,** 132-151.

Floriou-Servou, A., Von Ziegler, L., Stalder, L., Sturman, O., Privitera, M., Rassi, A., Cremonesi, A., Thöny, B. & Bohacek, J. 2018. Distinct proteomic, transcriptomic and epigenetic stress-responses in dorsal and ventral hippocampus. *Biological Psychiatry*.

Fox, M. D. & Raichle, M. E. 2007. Spontaneous fluctuations in brain activity observed with functional magnetic resonance imaging. *Nat Rev Neurosci,* 8**,** 700-11.

Fries, P., Neuenschwander, S., Engel, A. K., And, R. G. & Singer, W. 2001. Rapid feature selective neuronal synchronization through correlated latency shifting. *Nature Neuroscience* 4.

Fulcher, B. D. & Jones, N. S. 2017. hctsa: A Computational Framework for Automated Time-Series Phenotyping Using Massive Feature Extraction. *Cell Syst,* 5**,** 527-531 e3.

Fulcher, B. D., Little, M. A. & Jones, N. S. 2013. Highly comparative time-series analysis: the empirical structure of time series and their methods. *Journal of the Royal Society Interface,* 10(83).

Gao, R. & Penzes, P. 2016. Common Mechanisms of Excitatory and Inhibitory Imbalance in Schizophrenia and Autism Spectrum Disorders. *Curr Mol Med,* 15(2): 146–167.

Gomez, J. L., Bonaventura, J., Lesniak, W., Mathews, W. B., Sysa-Shah, P., Rodriguez, L. A., Ellis, R. J., Richie, C. T., Harvey, B. K., Dannals, R. F., Pomper, M. G., Bonci, A. & Michaelides, M. 2017. Chemogenetics revealed: DREADD occupancy and activation via converted clozapine. *Science,* 357**,** 503-507.

Grandjean, J., Preti, M. G., Bolton, T. a. W., Buerge, M., Seifritz, E., Pryce, C. R., Van De Ville, D. & Rudin, M. 2017a. Dynamic reorganization of intrinsic functional networks in the mouse brain. *Neuroimage,* 152**,** 497-508.

Grandjean, J., Zerbi;, V., Balsters;, J. H., Wenderoth;, N. & Rudin;, M. 2017b. Structural Basis of Large-Scale Functional Connectivity in the Mouse. *The Journal of Neuroscience* 37(34)**,** 8092-80=101.

Gray, C. M., Koenig, P., Engel, A. K. & Singer, W. 1989. Oscillatory responses in cat visual cortex exhibit inter-columnar synchronization which reflects global stimulus properties. *Nature* 338.

Grayson, D. S., Bliss-Moreau, E., Machado, C. J., Bennett, J., Shen, K., Grant, K. A., Fair, D. A. & Amaral, D. G. 2016. The Rhesus Monkey Connectome Predicts Disrupted Functional Networks Resulting from Pharmacogenetic Inactivation of the Amygdala. *Neuron,* 91**,** 453-66.

Greicius, M. D., Supekar, K., Menon, V. & Dougherty, R. F. 2009. Resting-state functional connectivity reflects structural connectivity in the default mode network. *Cereb Cortex,* 19**,** 72-8.

Griffanti, L., Salimi-Khorshidi, G., Beckmann, C. F., Auerbach, E. J., Douaud, G., Sexton, C. E., Zsoldos, E., Ebmeier, K. P., Filippini, N., Mackay, C. E., Moeller, S., Xu, J., Yacoub, E., Baselli, G., Ugurbil, K., Miller, K. L. & Smith, S. M. 2014. ICA-based artefact removal and accelerated fMRI acquisition for improved resting state network imaging. *Neuroimage,* 95**,** 232-47.

Gur, R. E. & Gur, R. C. 2010. Functional magnetic resonance imaging in schizophrenia. *Translational research* 12.

Hagmann;, P., Cammoun;, L., Gigandet;, X., Meuli;, R., Honey;, C. J., Wedeen;, V. J. & Sporns, O. 2008. Mapping the Structural Core of Human Cerebral Cortex *PLOS Biology,* 6(7).

Hahamy, A., Behrmann, M. & Malach, R. 2015. The idiosyncratic brain: distortion of spontaneous connectivity patterns in autism spectrum disorder. *Nat Neurosci,* 18**,** 302-9.

Haider, B. & Mccormick, D. A. 2009. Rapid neocortical dynamics: cellular and network mechanisms. *Neuron,* 62**,** 171-89.

Hasenstaub, A., Shu, Y., Haider, B., Kraushaar, U., Duque, A. & Mccormick, D. A. 2005. Inhibitory postsynaptic potentials carry synchronized frequency information in active cortical networks. *Neuron,* 47**,** 423-35.

Hu, H., Gan, J. & Jonas, P. 2014. Interneurons. Fast-spiking, parvalbumin(+) GABAergic interneurons: from cellular design to microcircuit function. *Science,* 345**,** 1255263.

Isaacson, J. S. & Scanziani, M. 2011. How inhibition shapes cortical activity. *Neuron,* 72**,** 231-43.

Iwabuchi, S. J., Krishnadas, R., Li, C., Auer, D. P., Radua, J. & Palaniyappan, L. 2015. Localized connectivity in depression: a meta-analysis of resting state functional imaging studies. *Neurosci Biobehav Rev,* 51**,** 77-86.

Just, M. A., Cherkassky, V. L., Keller, T. A., Kana, R. K. & Minshew, N. J. 2007. Functional and anatomical cortical underconnectivity in autism: evidence from an FMRI study of an executive function task and corpus callosum morphometry. *Cereb Cortex,* 17**,** 951-61.

Kahan, J., Urner, M., Moran, R., Flandin, G., Marreiros, A., Mancini, L., White, M., Thornton, J., Yousry, T., Zrinzo, L., Hariz, M., Limousin, P., Friston, K. & Foltynie, T. 2014. Resting state functional MRI in Parkinson's disease: the impact of deep brain stimulation on 'effective' connectivity. *Brain,* 137**,** 1130-44.

Kennedy, D. P. & Adolphs, R. 2012. The social brain in psychiatric and neurological disorders. *Trends Cogn Sci,* 16**,** 559-72.

Kraguljac, N. V., White, D. M., Hadley, N., Hadley, J. A., Ver Hoef, L., Davis, E. & Lahti, A. C. 2016. Aberrant Hippocampal Connectivity in Unmedicated Patients With Schizophrenia and Effects of Antipsychotic Medication: A Longitudinal Resting State Functional MRI Study. *Schizophr Bull,* 42**,** 1046-55.

Lazaro, M. T. & Golshani, P. 2015. The utility of rodent models of autism spectrum disorders. *Curr Opin Neurol,* 28**,** 103-9.

Leithner, C., Gertz, K., Schrock, H., Priller, J., Prass, K., Steinbrink, J., Villringer, A., Endres, M., Lindauer, U., Dirnagl, U. & Royl, G. 2008. A flow sensitive alternating inversion recovery (FAIR)-MRI protocol to measure hemispheric cerebral blood flow in a mouse stroke model. *Exp Neurol,* 210**,** 118-27.

Lewis, C. M., Bosman, C. A., Womelsdorf, T. & Fries, P. 2016. Stimulus-induced visual cortical networks are recapitulated by spontaneous local and interareal synchronization. *Proc Natl Acad Sci U S A,* 113**,** E606-15.

Lewis, D. A., Curley, A. A., Glausier, J. R. & Volk, D. W. 2012. Cortical parvalbumin interneurons and cognitive dysfunction in schizophrenia. *Trends Neurosci,* 35**,** 57-67.

Liska, A., Bertero, A., Gomolka, R., Sabbioni, M., Galbusera, A., Barsotti, N., Panzeri, S., Scattoni, M. L., Pasqualetti, M. & Gozzi, A. 2018. Homozygous Loss of Autism-Risk Gene CNTNAP2 Results in Reduced Local and Long-Range Prefrontal Functional Connectivity. *Cereb Cortex,* 28**,** 1141-1153.

M. G. Haberl, Valerio Zerbi, Andor Veltien, Melanie Ginger, Arend Heerschap & Frick, A. 2015. Structural-functional connectivity deficits of neocortical circuits in the Fmr1−/y mouse model of autism. *Science Advances,* 1500775.

Manvich, D. F., Webster, K. A., Foster, S. L., Farrell, M. S., Ritchie, J. C., Porter, J. H. & Weinshenker, D. 2018. The DREADD agonist clozapine N-oxide (CNO) is reverse-metabolized to clozapine and produces clozapine-like interoceptive stimulus effects in rats and mice. *Sci Rep,* 8**,** 3840.

Marissal, T., Salazar, R. F., Bertollini, C., Mutel, S., De Roo, M., Rodriguez, I., Muller, D. & Carleton, A. 2018. Restoring wild-type-like CA1 network dynamics and behavior during adulthood in a mouse model of schizophrenia. *Nat Neurosci,* 21**,** 1412-1420.

Mateo, C., Knutsen, P. M., Tsai, P. S., Shih, A. Y. & Kleinfeld, D. 2017. Entrainment of Arteriole Vasomotor Fluctuations by Neural Activity Is a Basis of Blood-Oxygenation-Level-Dependent "Resting-State" Connectivity. *Neuron,* 96**,** 936-948 e3.

Michaelides, M. & Hurd, Y. L. 2016. Chemogenetics: DREADDs. 2847-2856.

Mingshan, X., Bassam, V. A. & Massimo, S. 2014. Equalizing Excitation-Inhibition Ratios across Visual Cortical Neurons. *Nature* 511(7511)**,** 596-600.

Minshew, N. J. & Keller, T. A. 2010. The nature of brain dysfunction in autism: functional brain imaging studies. *Curr Opin Neurol,* 23**,** 124-30.

Mitra, A., Kraft, A., Wright, P., Acland, B., Snyder, A. Z., Rosenthal, Z., Czerniewski, L., Bauer, A., Snyder, L., Culver, J., Lee, J. M. & Raichle, M. E. 2018. Spontaneous Infra-slow Brain Activity Has Unique Spatiotemporal Dynamics and Laminar Structure. *Neuron,* 98**,** 297-305 e6.

Moore, A. K., Weible, A. P., Balmer, T. S., Trussell, L. O. & Wehr, M. 2018. Rapid Rebalancing of Excitation and Inhibition by Cortical Circuitry. *Neuron,* 97**,** 1341-1355 e6.

Nathanson, J. L., Yanagawa, Y., Obata, K. & Callaway, E. M. 2009. Preferential labeling of inhibitory and excitatory cortical neurons by endogenous tropism of adeno-associated virus and lentivirus vectors. *Neuroscience,* 161**,** 441-50.

Notter, T., Panzanelli, P., Pfister, S., Mircsof, D. & Fritschy, J. M. 2014. A protocol for concurrent high-quality immunohistochemical and biochemical analyses in adult mouse central nervous system. *Eur J Neurosci,* 39**,** 165-75.

Nucifora, F. C., Jr., Mihaljevic, M., Lee, B. J. & Sawa, A. 2017. Clozapine as a Model for Antipsychotic Development. *Neurotherapeutics,* 14**,** 750-761.

Oh, S. W., Harris, J. A., Ng, L., Winslow, B., Cain, N., Mihalas, S., Wang, Q., Lau, C., Kuan, L., Henry, A. M., Mortrud, M. T., Ouellette, B., Nguyen, T. N., Sorensen, S. A., Slaughterbeck, C. R., Wakeman, W., Li, Y., Feng, D., Ho, A., Nicholas, E., Hirokawa, K. E., Bohn, P., Joines, K. M., Peng, H., Hawrylycz, M. J., Phillips, J. W., Hohmann, J. G., Wohnoutka, P., Gerfen, C. R., Koch, C., Bernard, A., Dang, C., Jones, A. R. & Zeng, H. 2014. A mesoscale connectome of the mouse brain. *Nature,* 508**,** 207-14.

Okun, M. & Lampl, I. 2008. Instantaneous correlation of excitation and inhibition during ongoing and sensory-evoked activities. *Nat Neurosci,* 11**,** 535-7.

Paakki, J. J., Rahko, J., Long, X., Moilanen, I., Tervonen, O., Nikkinen, J., Starck, T., Remes, J., Hurtig, T., Haapsamo, H., Jussila, K., Kuusikko-Gauffin, S., Mattila, M. L., Zang, Y. & Kiviniemi, V. 2010. Alterations in regional homogeneity of resting-state brain activity in autism spectrum disorders. *Brain Res,* 1321**,** 169-79.

Packer, A. M. & Yuste, R. 2011. Dense, unspecific connectivity of neocortical parvalbumin-positive interneurons: a canonical microcircuit for inhibition? *J Neurosci,* 31**,** 13260-71.

Pagani, M., Bertero, A., Liska, A., Galbusera, A., Sabbioni, M., Scattoni, M. L., Pasqualetti, M. & Gozzi, A. 2018. Deletion of autism risk gene Shank3 disrupts prefrontal connectivity. *bioArchive*.

Penagarikano, O., Abrahams, B. S., Herman, E. I., Winden, K. D., Gdalyahu, A., Dong, H., Sonnenblick, L. I., Gruver, R., Almajano, J., Bragin, A., Golshani, P., Trachtenberg, J. T., Peles, E. & Geschwind, D. H. 2011. Absence of CNTNAP2 leads to epilepsy, neuronal migration abnormalities, and core autism-related deficits. *Cell,* 147**,** 235-46.

Rogan, S. C. & Roth, B. L. 2011. Remote control of neuronal signaling. *Pharmacol Rev,* 63**,** 291-315.

Roux, L. & Buzsaki, G. 2015. Tasks for inhibitory interneurons in intact brain circuits. *Neuropharmacology,* 88**,** 10-23.

Rubenstein, J. L. R. & Merzenich, M. M. 2003. Model of autism: increased ratio of excitation/inhibition in key neural systems. *Genes, Brain and Behavior***,** 255-267.

Safari, M. S., Mirnajafi-Zadeh, J., Hioki, H. & Tsumoto, T. 2017. Parvalbumin-expressing interneurons can act solo while somatostatin-expressing interneurons act in chorus in most cases on cortical pyramidal cells. *Sci Rep,* 7**,** 12764.

Scott-Van Zeeland, Brett S. Abrahams, Ana I. Alvarez-Retuerto, Lisa I. Sonnenblick, Jeffrey D. Rudie, Dara Ghahremani, Jeanette A. Mumford, Russell A. Poldrack, Mirella Dapretto, Daniel H. Geschwind & Bookheimer, S. Y. 2010. Altered Functional Connectivity in Frontal Lobe Circuits Is Associated with Variation in the Autism Risk Gene CNTNAP2. *Science Translational Medicine,* Vol 2 Issue 56 56ra80.

Selimbeyoglu, A., Kim, C. K., Inoue, M., Lee, S. Y., Hong, A. S. O., Kauvar, I., Ramakrishnan, C., Fenno, L. E., Davidson, T. J., Wright, M. & Deisseroth, K. 2017. Modulation of prefrontal cortex excitation/inhibition balance rescues social behavior in CNTNAP2-deficient mice. *Sci. Transl. Med.,* 9.

Selten, M., Bokhoven, H. V. & Kasri, N. N. 2018. Inhibitory control of the excitatory/inhibitory balance in psychiatric disorders. *F1000Research*.

Sethi, S. S., Zerbi, V., Wenderoth, N., Fornito, A. & Fulcher, B. D. 2017. Structural connectome topology relates to regional BOLD signal dynamics in the mouse brain. *Chaos,* 27**,** 047405.

Sforazzini, F., Bertero, A., Dodero, L., David, G., Galbusera, A., Scattoni, M. L., Pasqualetti, M. & Gozzi, A. 2016. Altered functional connectivity networks in acallosal and socially impaired BTBR mice. *Brain Struct Funct,* 221**,** 941-54.

Sohal, V. S., Zhang, F., Yizhar, O. & Deisseroth, K. 2009. Parvalbumin neurons and gamma rhythms enhance cortical circuit performance. *Nature,* 459**,** 698-702.

Tavor;, I., Jones;, O. P., Mars;, R. B., Smith;, S. M., Behrens;, T. E. & Jbabdi, S. 2018. Task-free MRI predicts individual differences in brain activity during task performance. *Science,* 352.

Uhlhaas, P. J. & Singer, W. 2006. Neural synchrony in brain disorders: relevance for cognitive dysfunctions and pathophysiology. *Neuron,* 52**,** 155-68.

Vogels, T. P., Sprekeler;, H., Zenke;, F., Clopath;, C. & Gerstner;, W. 2011. Inhibitory Plasticity Balances Excitation and Inhibition in Sensory Pathways and Memory Networks. *Science* 334.

Vogt, D., Cho, K. K. A., Shelton, S. M., Paul, A., Huang, Z. J., Sohal, V. S. & Rubenstein, J. L. R. 2017. Mouse Cntnap2 and Human CNTNAP2 ASD Alleles Cell Autonomously Regulate PV+ Cortical Interneurons. *Cereb Cortex*, 1-12.

Wang, S., Zhan, Y., Zhang, Y., Lyu, L., Lyu, H., Wang, G., Wu, R., Zhao, J. & Guo, W. 2018. Abnormal long- and short-range functional connectivity in adolescent-onset schizophrenia patients: A resting-state fMRI study. *Prog Neuropsychopharmacol Biol Psychiatry,* 81**,** 445-451.

Wilson, N. R., Runyan, C. A., Wang, F. L. & Sur, M. 2012. Division and subtraction by distinct cortical inhibitory networks in vivo. *Nature,* 488**,** 343-8.

Wohr, M., Orduz, D., Gregory, P., Moreno, H., Khan, U., Vorckel, K. J., Wolfer, D. P., Welzl, H., Gall, D., Schiffmann, S. N. & Schwaller, B. 2015. Lack of parvalbumin in mice leads to behavioral deficits relevant to all human autism core symptoms and related neural morphofunctional abnormalities. *Transl Psychiatry,* 5**,** e525.

Zang, Y., Jiang, T., Lu, Y., He, Y. & Tian, L. 2004. Regional homogeneity approach to fMRI data analysis. *Neuroimage,* 22**,** 394-400.

Zerbi, V., Grandjean, J., Rudin, M. & Wenderoth, N. 2015. Mapping the mouse brain with rs-fMRI: An optimized pipeline for functional network identification. *Neuroimage,* 123**,** 11-21.

Zerbi, V., Ielacqua, G. D., Markicevic, M., Haberl, M. G., Ellisman, M. H., A, A. B., Frick, A., Rudin, M. & Wenderoth, N. 2018a. Dysfunctional Autism Risk Genes Cause Circuit-Specific Connectivity Deficits With Distinct Developmental Trajectories. *Cereb Cortex,* 28**,** 2495-2506.

Zerbi, V., Ielacqua, G. D., Markicevic, M., Haberl, M. G., Ellisman, M. H., A-Bhaskaran, A., Frick, A., Rudin, M. & Wenderoth, N. 2018b. Dysfunctional Autism Risk Genes Cause Circuit-Specific Connectivity Deficits With Distinct Developmental Trajectories. *Cerebral Cortex.*

Zerbi, V., Jansen, D., Wiesmann, M., Fang, X., Broersen, L. M., Veltien, A., Heerschap, A. & Kiliaan, A. J. 2014. Multinutrient diets improve cerebral perfusion and neuroprotection in a murine model of Alzheimer's disease. *Neurobiol Aging,* 35**,** 600-13.